Laser and Particle Beams (1999), *vol.* 17, *no.* 3, *pp.* 427–435
Printed in the United States of America

2D high power laser diode arrays for solid-state laser driver inertial fusion energy project

By N.G. BASOV, Yu.M. POPOV, V.V. BEZOTOSNY, and Kh.Kh. KUMYKOV
Lebedev Physical Institute, 53 Leninsky Prospect, 117924 Moscow, Russia

(Received 4 July 1998; Accepted 6 November 1998)

2D arrays of laser diodes were developed and investigated under QCW operating conditions. Output power and energy density up to 1 kW/cm^2 and 0.45 J/cm^2 (at pulse duration 0.5 ms) were measured at the wavelength 810 nm. The spectral composition of radiation, shape of the output pulses, and far-field and near-field radiation zones were examined under various pumping parameters. The kinetics of the temperature profiles in monolithic QCW AlGaAs/GaAs linear bars and 2D arrays, emitting at the wavelength 810 nm was modeled numerically. Quasi-CW and CW operation under various pump parameters were considered as a function of a heat sink design. A calculation model was used to interpret the experimental dependences of the output parameters of the arrays on the pump conditions for application in the solid-state laser driver project. The limit of total power conversion efficiency of diode lasers was analyzed in respect of the threshold current density, series resistance and external differential quantum efficiency. The estimated maximum value of 75% was obtained for the present technological level of the diode lasers production. The corresponding limit of the output optical power density of 2D laser array was defined around 10 kW/cm^2.

1. Introduction

It is well known that the process of inertial laser fusion would be effective if the efficiency of an induced high-power laser is not less than 10% (this is, of course, a conventional figure, but quite real). Note that the efficiency of all the existing high-power solid-state lasers pumped by a flash-lamp is considerably lower. That is why all the existing, most powerful laser fusion facilities are destined only for the model experiments, and can by no means be used as the basis for future power stations. Strange as it may seem, the destiny of most of the high-power fusion laser facilities turned out to be dependent on the small-size and low-power diode lasers. Such advantageous characteristics of a diode laser as high output efficiency achieving 70%, and a feasibility of total absorption of a narrow-band radiation by an active element of a laser material, provide pumping of a high-power laser (or several lasers) destined for inertial fusion with total efficiency of about 10%, or it may be higher. A comparatively low power of a separate diode laser is compensated by its small size (which is an exceptionally favorable feature for the integral technologies). So the total light flow is radiated from an area comparable with a pumped area of a high-power laser (one can provide a ten-fold optical concentration).

A future power station using a fusion laser will operate in a pulse-periodic regime. If an output power of a station is planned to be around 1 GW (and further we shall use this very figure) then it will be needed to use from 5 to 10 laser pulses, each of about 3 MJ energy to be input into a target during a pulse, provided that the input energy is amplified by a target by about 70–100 times. As a result, the whole system, including the pumping, will operate in a pulse-periodic regime of not higher than 10–20 Hz frequency. It is known that the difference in

 0263-0346/99 $12.50

the radiated power during the continuous and pulse-periodic operations is not as high for diode lasers as for other types of pumping lasers. However, requirements for an outlet of high power for the case of 2D matrices at 10–20 Hz operation influence considerably the power and operation stability of a matrix during a working cycle which ranges from 0.2 to 1 ms under pumping of most known active materials.

We shall speak about such times of the diode laser radiation at higher power densities. It is commonly accepted now that the limit power of the best diode laser at pulse duration above ten nanoseconds is determined by a particular material that is used near the boundary of an output mirror radiation. This limit power does not exceed 10 MW/cm^2 for the acceptable lifetime of a GaAs diode laser. This figure should be taken into account when considering maximal radiation power of an element. All the rest of the factors going from the surface of a laser diode, like passive areas of a diode, substrates, contacts, cooling systems, etcetera, will only reduce this value. As a result, this figure will be reduced by 10^4 times (at most, 10^3 times) for 2D laser batteries, and will lead to 10^4 W/cm^2 limit power. The power of high-quality 1D arrays and 2D batteries is limited by heat transfer which does not allow an exceeding temperature of an active region by a few tens degrees.

In order to show vividly the picture of heat transfer it is necessary to consider a 1D thermal model. Let us assume some unlimited area along $p-n$ junction with a thermal power which is dissipated in the direction normal to this plane in x-direction. Of course, there is quite a variety of the material layers in this direction.

2. Thermal model

A steady-state thermal model of a linear array of semiconductor lasers was considered by Nakwaski (Mroziewicz *et al.* 1991). This model can be used to calculate the inhomogeneity of the steady-state temperature distributions in the $p-n$ junction plane. The kinetics of temperature changes were also considered by Nakwaski, but only in the approximation of short pulses (<0.5 μs), so that these results cannot be extended to analyze quasi-*cw* transient conditions.

3. 1D Thermal model

We considered a GaAs/AlGaAs double heterostructure with a separate confinement of electrons and photons, and emitting at a wavelength of 0.81 μm. It is assumed that this heterostructure is mounted on a heat sink and soldered to it with indium, Pb-Sn, or other alloy. Double-sided bounding assembly is assumed because it can be used to simulate single-sided (from each of the sides) or double-sided removal of heat from a linear laser array. The temperature distribution in the layers is described by the transient heat conduction equation:

$$C(x)\rho(x)\frac{\partial T}{\partial t} = \frac{\partial}{\partial x}\left\{k(x)\frac{\partial T}{\partial x}\right\} + P(x,t), \tag{1}$$

with boundary conditions

$$\left[\alpha_1(t)\frac{\partial T}{\partial x} + \beta_1(t)T - \gamma_1(t)\right]_0 = 0$$

$$\left[\alpha_2(t)\frac{\partial T}{\partial x} + \beta_2(t)T - \gamma_2(t)\right]_L = 0, \tag{2}$$

$C(x)$—specific heat, $\rho(x)$—crystal density, $k(x)$—thermal conductivity, $P(x,t)$—the density of heat sources, α, β, γ—are time-dependent coefficients governed by the heat-exchange conditions; the coordinate x is directed perpendicular to the heterostructure layers and varies from zero to L. The thermal parameters of the SCH and heat sinks are presented in table 1.

https://doi.org/10.1017/S0263034699173105 Published online by Cambridge University Press

TABLE 1. Parameters of the materials used in calculations of thermal conditions in linear laser arrays based on AlGaAs/GaAs heterostructures.

Laser structure component	Material	Thickness/μm	Thermal conductivity/ W m^{-1} K^{-1}	Specific heat/ J g^{-1} K^{-1}	Density/g cm^{-3}
Heat sink	Cu	100–5000	401	0.38	8.96
	BeO	100–5000	230	1	3.01
Solder	Sn	1–10	67	0.23	7.29
	In	1–10	82	0.23	7.31
Substrate	GaAs	80	44	0.32	5.32
Emitter	$Al_{06}Ga_{04}As$	1.4	12	0.4	4.36
Waveguide	$Al_{02}Ga_{06}As$	0.14	11	0.37	4.68
Active region	$Al_{01}Ga_{09}As$	0.01–0.05	20	0.33	5.16

Assumptions:

1. Structure is unbounded in the $p-n$ junction plane,
2. $C(x)$, $\rho(x)$, $k(x)$, and $P(x,t)$ are independent of temperature,
3. $P(x,t)$ is independent of coordinates y and z,
4. Heat sources are uniformly distributed in the active layer.

For a multilayer plate, equation (1) is transformed to the system of equations:

$$\frac{\partial T_i}{\partial t} = a_i \frac{\partial^2 T_i}{\partial x^2} + f_i$$
$$a_i = \frac{k_i}{C_i \rho_i}; \qquad f_i = \frac{P_i}{C_i \rho_i}; \qquad i = 1,\ldots n \tag{3}$$

where k_i, C_i, ρ_i are the parameters that apply to the ith layer; P_i is the density of heat sources in the ith layer.

Four types of heat exchange at the outer boundaries were analyzed:

1. Constant temperature of the outer boundary
2. Constant heat flux at the outer boundary
3. The absence of the heat exchange at the outer boundary
4. Heat sink of the infinite thickness

The dynamics of the temperature profiles in the laser bar is shown in figure 2.

The following results are of practical interest:

- Non-symmetricity of the temperature profiles in one-side and also two-side bonded structures.
- Saturation of the temperature at the outer boundary substrate-air at pulsewidths around 1 ms.
- The influence of the solder material (In, Sn, Pb-Sn, etc.) and its thickness is small (in thickness range 1–10 mkm around 0.5–3.5°C).
- The material of the heat sink plays the main role in active layer temperature rise T_{max} and temperature distribution in the laser crystal: replacement of BeO on Cu lowers T_{max} from 45°C to 35°C (assumed low duty factor and pulse duration 1 ms, initial temperature 0°C). Under CW operation, replacement of BeO with Cu has an greater effect, T_{max} decreases from 68°C to 42°C. For diamond heat sink with thermal conductivity 1000 W/mK, T_{max} is only 19°C, (all the data for 1 cm laser bar with thermal load 100 W/cm).

https://doi.org/10.1017/S0263034699173105 Published online by Cambridge University Press

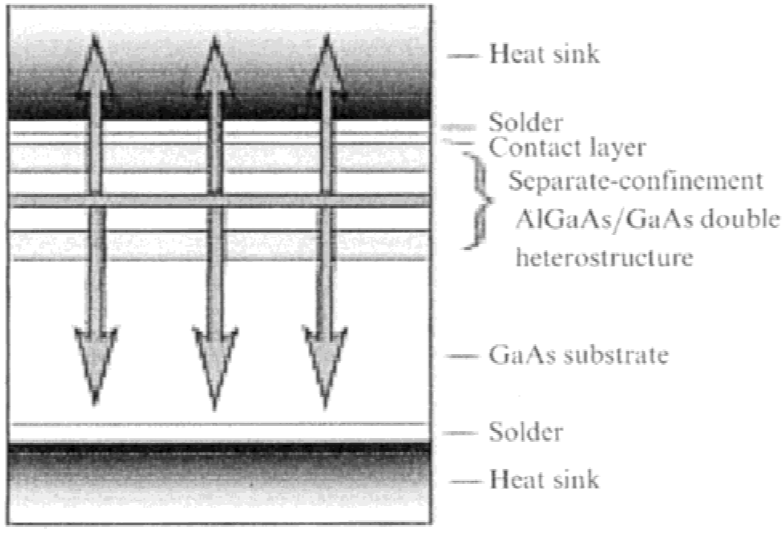

FIGURE 1. Schematic representation of SCH AlGaAs/GaAs structure with double-sided heat removal. The arrows show the direction of heat flow from the active layer to heat sinks.

- The effect of double-sided heat removal (in comparison with one-sided) is more for heat-sink materials with low thermal conductivity (for example 0.4 mm thick diamond heat sink lowers T_{max} by 4.5°C, Cu by 8°C, BeO by 23°C.
- The material of the heat sink from the substrate side of the structure is less important than from the active layer side due to the low thermal conductivity of the semiconductor heterostructure: with diamond $\Delta T_{max} = 5$°C, with Cu—4.7°C and with BeO—4°C (thickness of the heat sink from the substrate side is 50 μm, substrate thickness 80 μm).
- Heat sink from the substrate side is very useful when thermal conductivity of the main heat sink is low (BeO, CuW, CuMo, etc.).
- The influence of the heterostructure thickness is substantial. For substrate thickness range $d_{sub} = 20$–180 mkm and one-side heat sink $T_{max} = 47$–38°C. The addition of 50 mkm Cu heat sink from the substrate side reduces the active layer temperature rise to $T_{max} = 40$–36.5°C.

The kinetics of the temperature profiles is shown at figure 3.

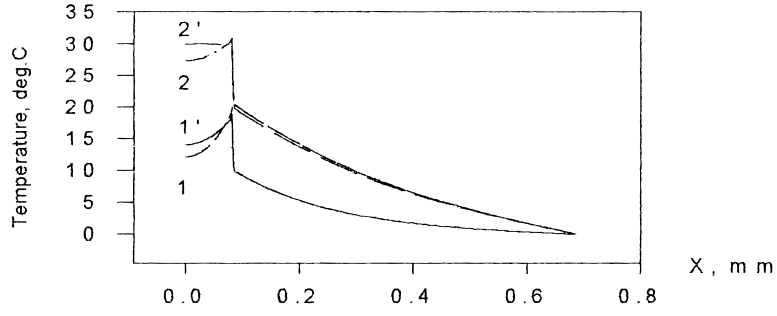

FIGURE 2. Transverse temperature distribution in a laser bar. Duration of current pulses 0.25 ms (1,1′) and 0.5 ms (2,2′). Curves 1,2—heat sources confined only to the active layer. Curves 1′,2′—take account also of the Joule losses and SE absorption.

https://doi.org/10.1017/S0263034699173105 Published online by Cambridge University Press

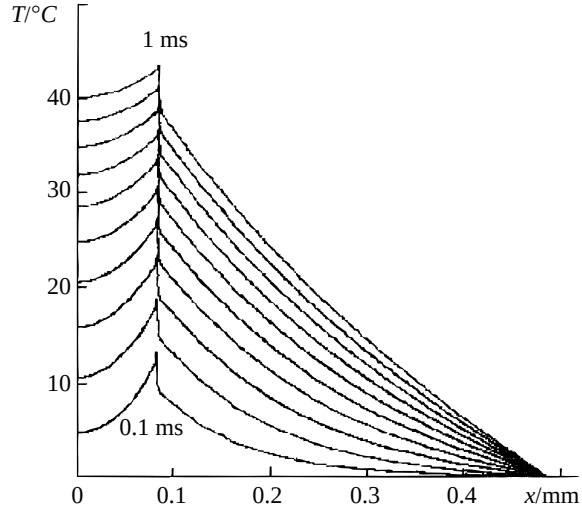

FIGURE 3. Temperature profiles for a 0.4 mm thick BeO heat sink in the absence of heat exchange at the substrate-air interface (on the left) and for $T = 0$ (on the right). The time interval is 0.1 ms and thermal load 120 W/cm^{-1}.

The duty factor influence on the temperature dynamics of the array is illustrated by figure 4. At low duty-cycle operation regime (figure 4a), the array is working at thermocycle-type conditions. At high duty factor (figure 4b), the thermocycling effect is less, but the maximum and the average temperature of the laser array is more, so it is not easy to guarantee the lifetime and reliability of the device in both cases.

4. 2D Thermal model

In order to investigate spatial heat-spreading effects in 2D diode-laser arrays we developed a 2D thermal model. Laser array consists of the set of sections, subassemblies (figure 5).

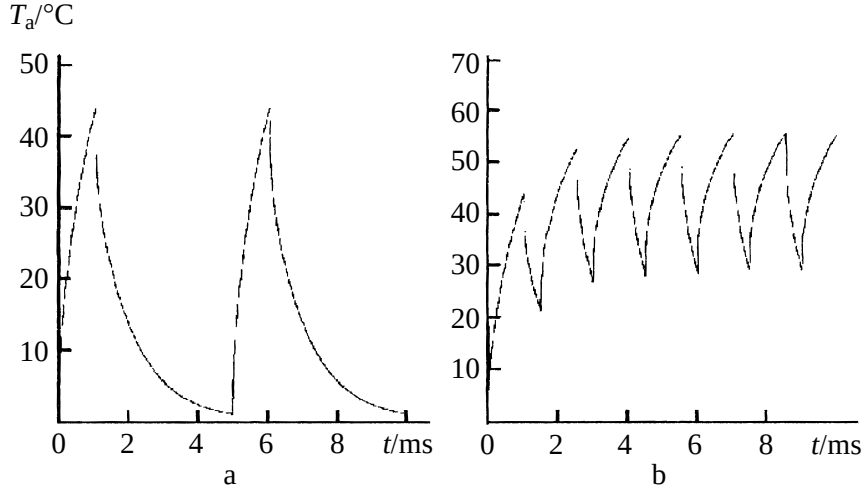

FIGURE 4. Calculated time dependence of the temperature of the active region expected for the pulses of 1 ms duration and a repetition period of 5 ms ((a) small duty factor) and 1.5 ms ((b) high duty-factor). The other parameters are the same as in figure 3.

https://doi.org/10.1017/S0263034699173105 Published online by Cambridge University Press

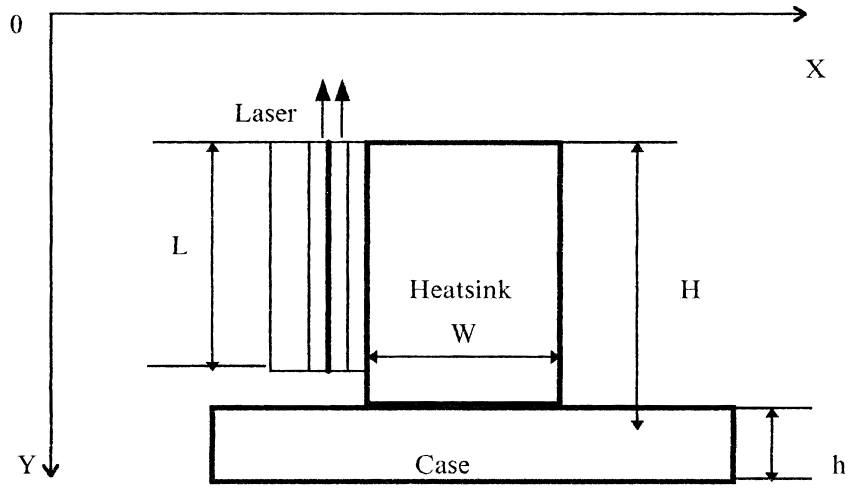

FIGURE 5. Laser bar subassembly.

Sections are thermally connected within the common water-cooled case and air gaps. Simulation shows that due to high thermal conductivity of the case material and low thermal conductivity of the air, at QCW operation each subassembly can be treated as thermally isolated. Hence, it is sufficient to study the dynamics of heat spreading in one separate section. We treated laser-diode structure, described earlier accounting for size and shape of the subassembly and thermal properties of the environment. The new useful information from the results of 2D model is the value of temperature variation along the resonator length. At usual thermal loads it can be 20% and even 30% according to the maximum overheating, so that must be accounted in the adequate modeling of the main parameters of CW and QCW diode lasers.

The temperature distribution in the layers and in the heat sink is described by the 2D transient heat conduction equation:

$$C(x,y)\rho(x,y)\frac{\partial T}{\partial t} = \frac{\partial}{\partial x}\left\{k(x,y)\frac{\partial T}{\partial x}\right\} + \frac{\partial}{\partial y}\left\{k(x,y)\frac{\partial T}{\partial y}\right\} + P(x,y,t), \tag{4}$$

with boundary conditions similar to equation (2) in both dimensions. Equation was solved with finite difference method for multielement media. Solving equation (3) and comparing the results with the data of the 1D model we found that 1D model adequately describes temperature profiles in a crosssection perpendicular to the active layer, and can be used to evaluate the upper limit of the temperature distribution. The new information from the results of 2D model calculations is more precise temperature distribution in the subassembly including the considerable variation of the temperature along the laser resonator axis (figure 6) and air heating besides the subassembly.

5. Total efficiency of diode lasers

The total efficiency of a laser diode η_t (sometimes called the wall-plug efficiency) is the ratio of the total optical power P_{opt} to the total electrical power P_{el} reaching a laser crystal:

$$\eta_t = \frac{P_{opt}}{P_{el}} \approx \eta_d \frac{(I - I_{th})\cdot E_g}{I[U_t + R_s(I - I_{th})]}, \tag{5}$$

where E_g is the band gap in volts, R_s is the series resistance of a laser diode, U_t is the voltage across a diode at the lasing threshold, and η_d is the external differential quantum efficiency.

https://doi.org/10.1017/S0263034699173105 Published online by Cambridge University Press

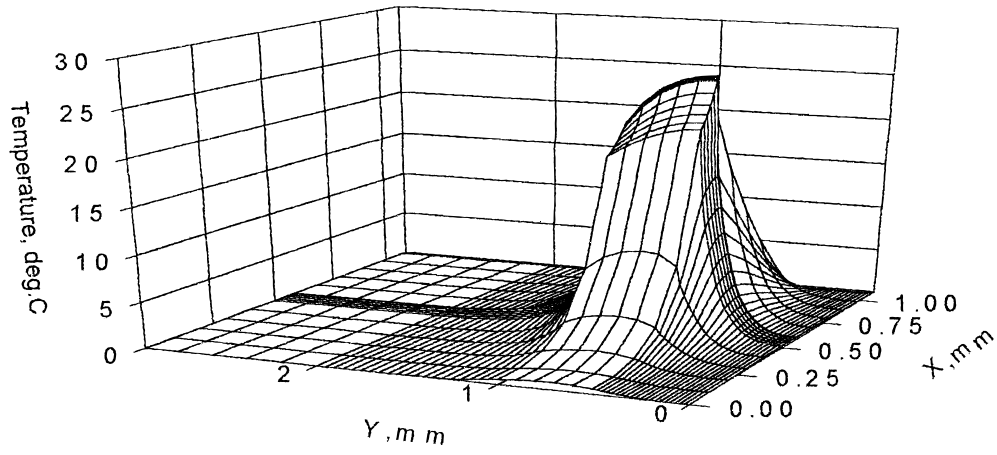

FIGURE 6. 2D laser array subassembly temperature profile. Cu—Heat sink, $H = 1.5$ mm, $W = 0.5$ mm, $L = 0.5$ mm.

The internal quantum efficiency of the heterostructures and laser diodes developed so far is $\eta_i \approx 0.95$. Antireflection and reflecting coatings of the facet mirrors ensure that the reflection coefficients are $R_1 \approx 5\%–10\%$ and $R_2 \approx 93\%–97\%$, so that for a cavity $L = 500$ mkm long and for $\alpha_I = 4–1$ cm^{-1}, the range of η_d is $0.8 \leq \eta_d \leq 0.9$. The maximum η_t^{max} and current I_{max}, at which it is reached amounts to:

$$\eta_t^{max} = \frac{\eta_d \cdot C \cdot E_g}{(I_{th} + C)(U_t + R_s C)}, \qquad I_{max} = I_{th} + C, \qquad C = \sqrt{\frac{I_{th} \cdot U_t}{R_s}}. \tag{6}$$

The results of calculations of η_t^{max} for $\eta_d = 0.8$ and 0.9 when $R_s = 0.01–0.001\ \Omega$ are given in figure 5 for bars with the cavity 500 mkm long and 1 cm wide.

The experimental symbols at figure 8 are our experimental results (○,◇) and adapted results from Mawst (1996)—(□) and O'Brien *et al.* (1996) and SDL Product Catalog (1997)—(×). Even when the threshold current density is fairly high (500 A/cm^2), the total efficiency η_t^{max} can be high (up to 65%) if the series resistance of a bar is reduced to $10^{-3}\ \Omega$. On the other hand, when the threshold current density is at its low limit (100 A/cm^{-2}), η_t^{max} does not exceed 40%–45% if the series resistance is $10^{-2}\ \Omega$ (Bezotsonyii *et al.* 1995).

On the base of our thermal model, we propose the design of the laser bar, which ensures the output power up to the limit of the catastrophical optical damage to the mirrors. The main features of that design are: heat sink from the synthetic diamond, two-side (from the epilayers and from the substrate) heat removal, and thinner than usual substrate of the heterostructure. The calculated heat distribution in the laser bar, mounted at such submount at thermal load six times more than at figure 1 is shown in figure 7.

6. Results and discussion

1D and 2D numerical thermal models of the laser bar and array were developed. The main experimental results on output parameters of the laser bars and arrays are appropriately described by these models. Predicted maximum total efficiency of the diode lasers is around 75%

https://doi.org/10.1017/S0263034699173105 Published online by Cambridge University Press

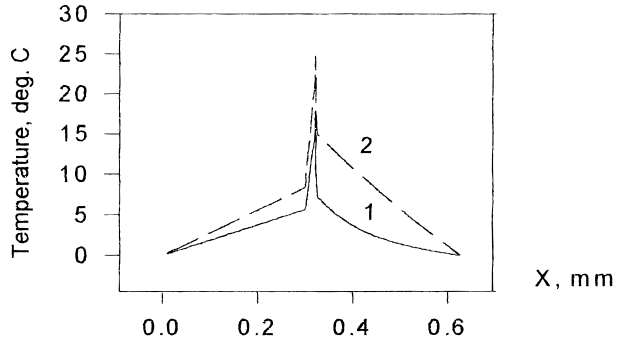

FIGURE 7. Transverse temperature distribution in laser bar with double-side heat sink. Diamond heat sink is 0.3 mm thick, pulsewidths (1) 0.1 ms and (2) 0.5 ms.

in accordance with current experimental results. The proposed design of the laser bar, two-side, mounted at the diamond heat sinks ensures the increase of the maximum output power from the single laser bar up to the 1 kW/cm, which is close to the COD level. Estimated maximum output optical power (Botez *et al.* 1996) of the 1 cm^2 2D laser diode array is ≈10 kW.

The detailed temperature profiles and design parameters of the arrays at wavelengths 808 nm and 940 nm for efficient pumping of correspondingly Nd:YAG and Yb:YAG solid-state laser materials, which are used in the highest power lasers at LLNL, TRW, and Hughes Aircraft with diode pumping were presented in Bezotosny & Kumykov (1998).

The total efficiency of the pumping system for the energy power station is one of the key parameters. The best up to date total efficiency, obtained for 980 nm wavelength lasers is 0.59–0.66 (Botez *et al.* 1996; Garbuzov *et al.* 1997). We believe that our result of 0.5 for room-temperature total efficiency of CW 808 nm lasers (Bezotosny *et al.* 1998) is one of the best.

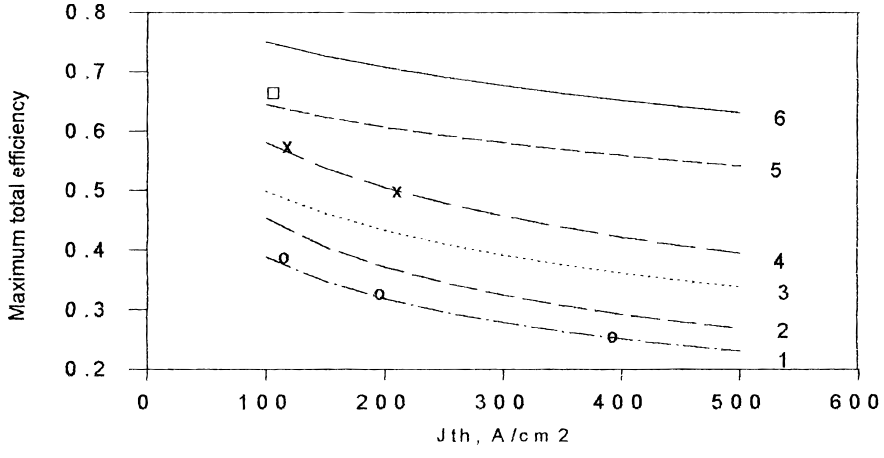

FIGURE 8. Calculated maximum efficiency of laser bar: *Rs* = 0.01 Ohms (1,2); *Rs* = 0.005 Ohms (3,4), and 0.001 Ohms (5,6); diff. efficiency 0.8 (1,3,5), 0.9 (2,4,6).

https://doi.org/10.1017/S0263034699173105 Published online by Cambridge University Press

Acknowledgment

This work was supported by the council of grants of the president of Russia and state support of the leading scientific schools 96-15-96596.

REFERENCES

Adlivankin, A.S. *et al.* 1996 *Kvantovaya Elektron.* (Moscow), **23**, 974. [*Quantum Electron* **26**, 949 (1996)].

Bezotsonyiï, V.V. *et al.* 1995 *Kvantovaya Elektron.* (Moscow), **22**, 101. [*Quantum Electron* **25**, 93 (1995)].

Bezotsonyiï, V.V. *et al.* 1996 *Kvantovaya Elektron.* (Moscow), **23**, 775. [*Quantum Electron* **26**, 755 (1996)].

Bezotsonyiï, V.V. *et al.* 1997 *Kvantovaya Elektron.* (Moscow), **24**, 6. [*Quantum Electron* **27**, 6 (1997)].

Bezotosny, V.V. *et al.* 1998 *Quantum Electron* **25**, 4.

Bezotosny, V.V. & Kumykov, Kh.Kh. 1998 *Quantum Electron.* **28**, 3.

Botez, D. *et al.* 1996 *Electron. Lett.* **32**, 2012.

Garbuzov, D.Z. *et al.* 1997 *Electron. Lett.* **33**, 1462.

Mawst, L.J. *et al.* 1996 *Appl. Phys. Lett.* **69**, 1532.

Mroziewicz, B. *et al.* 1991 *Physics of Semiconductor Lasers* (Warsaw: PWN).

O'Brien, S. *et al.* 1996 *Proceedings of the 9th Annual Meeting of the Lasers and Electro-Optics Society,* (LEOS'96) (Boston, MA) Postdeadline paper 13.

SDL Product Catalog 1996/1997 (San Jose CA: SDL Inc., 1996).